A Reliable Generation Method for Reference Orbit of Precise Repeat-Track Orbit

Zhe Xu[(1)], Jianjun Feng[(1)], Xingke Fu[(1)], Hua Cui[(1)]

[(1)] Zhuzhou Space Interstellar Satellite Technology Co., Ltd.
Shanghai, China
Email: xz120202@gmail.com

***Abstract* – This paper presents a highly reliable generating method for Precise Repeat-Track (PRT), driven by interferometric mapping applications of Synthetic Aperture Radar (SAR) satellite system. Under highly nonlinear high-order perturbation, design optimization process employing traditional numerical gradient methods or convex optimization approaches may encounter issues of unstable convergence in results. To address this issue, this paper introduces an adaptive search strategy with superior adaptability, providing increased flexibility to effectively address the complex response distribution. The proposed method not only circumvents the computational challenges posed by global optimization but also mitigates the limitations of numerical gradient optimization. This method enhances the reliability of convergence, providing assurance for the rapid and dependable on-orbit redesign requirements in practical missions. Simulation demonstrates advantages of the proposed design method in both computational efficiency and convergence success rate, while ensuring convergence accuracy.**

I. INTRODUCTION

The Nüwa constellation is China's first large-scale commercial remote satellite constellation. The initial phase of the plan consists of 54 satellites, including 44 SAR satellites. In the later stages, the plan aims to expand to approximately 200 satellites. Four satellites, among them, have been launched in 2023 and are currently operational in orbit. The SAR satellites within this constellation are designed to have the capability of Differential Synthetic Aperture Radar interferometry (D-InSAR). This requires the satellite to achieve high-precision regression in the three-dimensional space of the Earth-fixed frame. Therefore, orbital design must ensure that the Earth-fixed trajectory of the orbit seamlessly connects at the beginning and the end within a single regression cycle. Missions such as Terra-SAR, ALOS, Sentinel, etc., have adopted the PRT designs [1,2,3,4,5]. Among these, the classical design method proposed by D'Amico, etc., has been widely adopted and referenced. In the classical method, the design architecture introduces at least 2 additional "virtual maneuvers", bringing the total number of design variables up to 14, along with the introduction of 12 constraints [6]. As a result, during the optimization process, there is a tendency to fall into local optimum too early, while success of convergence is influenced by initial conditions and hyperparameters. Later researchers have proposed various design methods within direct shooting framework, including GA, NSGA-II, differential correction, gradient descent, etc. Under high-order perturbations, the strong non-linear characteristics of the problem result in the objective function presenting noise-like distribution characteristics at small scales. Heavily relying on gradient matrix or Jacobian matrix, traditional numerical gradient methods and optimizers based on linear regression often struggle to acquire effective gradient information, resulting in convergence failures. In practical engineering, especially in commercial missions, there is often a requirement to promptly enter the "control tube" defined about a PRT shortly after the satellite is placed in orbit. This necessitates redesigning of the PRT based on the actual orbital conditions to avoid unnecessary orbital adjustments. Therefore, it is essential to establish an efficient and reliable optimization design process to ensure convergence without manual intervention.

In this paper, comprehensive design approach that meets the previously mentioned requirements is discussed. The proposed method essentially inherits the widely adopted multi-stage design architecture. Semimajor axis and inclination are defined as the design variables in this work. In the discussion of the "Regression Refinement" stage, distributions of the response for objective function are plotted, considering high-order non-spherical perturbations, based on which non-smooth behaviour in the distribution is illustrated. This raises the numerical computation issues of the gradient matrix faced by traditional gradient methods. To address the decrease in convergence reliability caused by this issue, an adaptive optimization design approach is incorporated into the Newton's method and employed in terms of multi-round iteration. On the other hand, this work presents the fact that achieving precise regression over an integer number of days inherently satisfies sun-synchronous characteristic. Hence, the "SSO Refinement" stage is integrated into other stage. Next, a considerable number of simulation cases are carried out under various design conditions. All cases get convergence reliably, ensuring that the state difference between the initial and final points of each cycle in Earth-fixed coordinate system is within 1 meter. Finally, the convergence characteristics of the proposed method are compared with traditional derivative-information-

based optimization approach. The comparative results indicate that this method presents significantly better convergence success rates compared to traditional local optimization methods and achieves considerably faster convergence compared to global optimization.

II. Problem Description

In some classical methods, the design process of PRT is often described as [6]

design: $[\bar{a}_0 \quad \bar{\imath}_o]$
objective: minimize $\delta P = |\mathbf{P}_t - \mathbf{P}_0|$
subject to: Sun-synchronous constraint

in which, $\bar{a}_0$, $\bar{\imath}_o$ are the mean orbital elements of the semi-major axis and inclination at the initial epoch, respectively. $\mathbf{P}_0$ represents the expression of the initial orbital position vector in the Earth-Fixed frame (WGS-84). $\mathbf{P}_t$ is the position vector in the Earth-Fixed frame at time t, where t is one regression period. δP is the discontinuity between the two."

By optimizing the mean elements of the semi-major axis and inclination, the discontinuity between the initial position in the Earth-Fixed frame and its final position after one regression period is minimized. Typically, this discontinuity is required to be less than 1 meter, which is a commonly adopted design standard in practical engineering tasks.

Given $\mathbf{P}_0$, $\mathbf{P}_t$ is obtained through numerical integration with an integral duration of one regression period, using a standard Earth non-spherical gravitational perturbation model such as EGM2008 or GGM01. Other perturbations, such as third-body, solar radiation pressure, atmospheric drag, etc., are not considered. This is because these perturbations are typically of small magnitude and cannot be accurately predicted in practice; therefore, they are generally treated as unknown perturbations during the precise orbital control about the “tube”.

In the practical design process of PRT, no matter how the mean semi-major axis $\bar{a}_0$ and the mean inclination $\bar{\imath}_o$ are improved (written as the "Regression Improvement" in below), convergence accuracy of only kilometer level can be achieved. This is because the orbital frozen condition is not fulfilled. Specifically, at this stage, $\mathbf{P}_0$ and $\mathbf{P}_t$ can only coincide in the horizontal direction in terms of longitude and latitude, while there exists a significant difference in the altitude direction. Therefore, it is necessary to introduce a frozen orbit refinement phase. This phase can be conducted independently from the regression refinement phase mentioned above. Subsequently, by carrying out the second regression improvement phase, the discontinuity δP can get converged to the required accuracy. Hence, a classical optimization structure with three independent stages is formed.

III. Problem Analysis

A. Non-linear Problem Characteristics

In ideal circumstances, the two regression improvement phases among the three-stage optimization structure, can be conducted employing optimization methods dependent on gradient information, e.g., differential corrections and Newton's method. The use of gradient methods necessitates the repeated calculation of Jacobian matrices and sometimes Hessian matrices. This requires accurate and reliable computational result. Numerical method is the most common way to compute partial derivative matrices. The formulas for calculating the Jacobian and Hessian matrices of a binary function are given by the following equations:

$$\nabla f = \begin{bmatrix} f_x(x_0, y_0) \\ f_y(x_0, y_0) \end{bmatrix} = \begin{bmatrix} \frac{\partial f}{\partial x} \\ \frac{\partial f}{\partial y} \end{bmatrix} = \begin{bmatrix} \frac{f(x_0+h, y_0)-f(x_0 y_0)}{h} \\ \frac{f(x_0, y_0+h)-f(x_0, y_0)}{h} \end{bmatrix} \tag{1}$$

$$\nabla^2 f = \begin{bmatrix} f_{xx}(x_0, y_0) & f_{xy}(x_0, y_0) \\ f_{yx}(x_0, y_0) & f_{yy}(x_0, y_0) \end{bmatrix} = \begin{bmatrix} \frac{\partial f_x}{\partial x} & \frac{\partial f_x}{\partial y} \\ \frac{\partial f_y}{\partial x} & \frac{\partial f_y}{\partial y} \end{bmatrix} = \begin{bmatrix} \frac{f_x(x_0+h, y_0)-f_x(x_0, y_0)}{h} & \frac{f_x(x_0, y_0+h)-f_x(x_0, y_0)}{h} \\ \frac{f_y(x_0+h, y_0)-f_y(x_0, y_0)}{h} & \frac{f_y(x_0, y_0+h)-f_y(x_0, y_0)}{h} \end{bmatrix} \tag{2}$$

where h is a small quantity, typically ranging from 10^{-6} to 1×10^{-8}, in units of km or rad depending on specific problems. For continuous and smooth surfaces or curves, such calculations are often feasible. However, for non-smooth surfaces or curves, incorrect results may arise. Fig. *1* illustrates the situation of derivative calculation on a non-smooth curve, which can be extended to higher dimensions. As shown in the figure, if high-frequency effects are neglected, $\nabla f < 0$ and $\nabla^2 f > 0$ should be determined on the focusing position. However, due to the presence of oscillations, the algorithm based on (1) and (2) may lead to uncertain

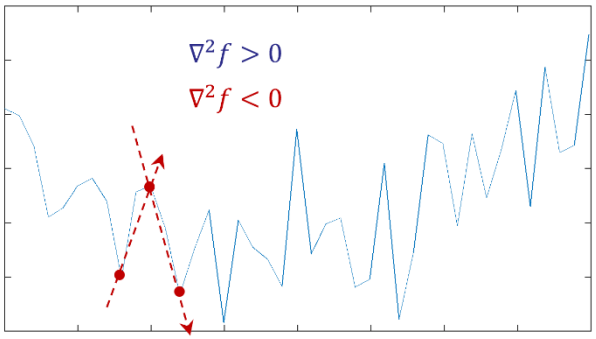

Fig. *1. Explanation for Calculation Defects of Derivatives on Unsmooth Distribution Surface/Curve*

results, as indicated by the red dashed lines and arrows in the figure. They result in either ∇f<0 or ∇f>0. As the result, the calculation yields $\nabla^2 f < 0$ in this example. It is easy to understand that such results have a significant negative impact on the convergence process of gradient optimization methods.

As mentioned in the previous section, the core issue of the improvement phase can be seen as an optimization problem of the binary function $\delta P = f(\bar{a}_0, \bar{\imath}_o)$. (Note: For simplicity, $\bar{a}_0$ and $\bar{\imath}_o$ will be denoted as a and i in below). Investigation focuses on the distribution of the objective value δP with respect to a and i. Fig. 2 illustrates a case of 2×0 (degree×order) non-spherical perturbation. The surface distribution in the figure appears smooth and thus suitable for gradient methods. Investigation found that this surface distribution also presents smoothness at a small scale.

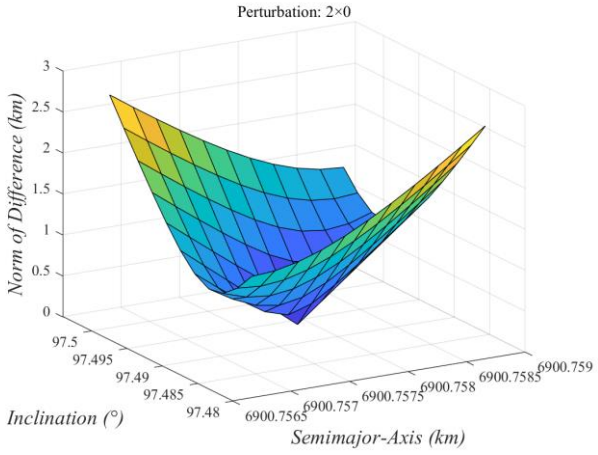

Fig. 2. Distribution Surface under 2 ×0 Perturbation

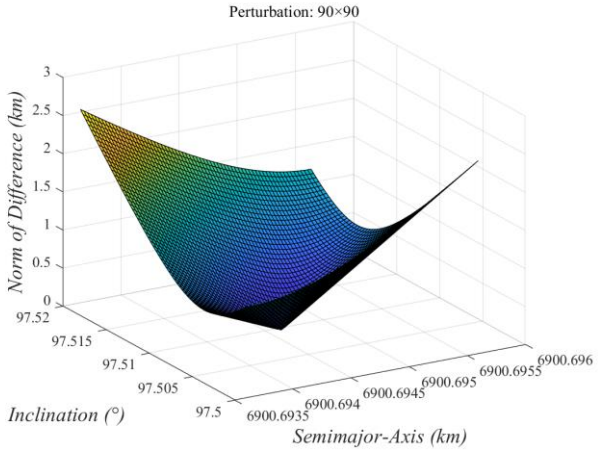

Fig. 3. Distribution Surface under 90 ×90 Perturbation

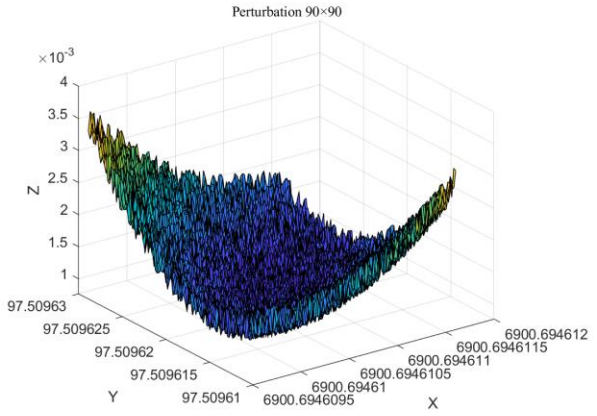

Fig. 4. Distribution Surface under 90 ×90 Perturbation (zoomed)

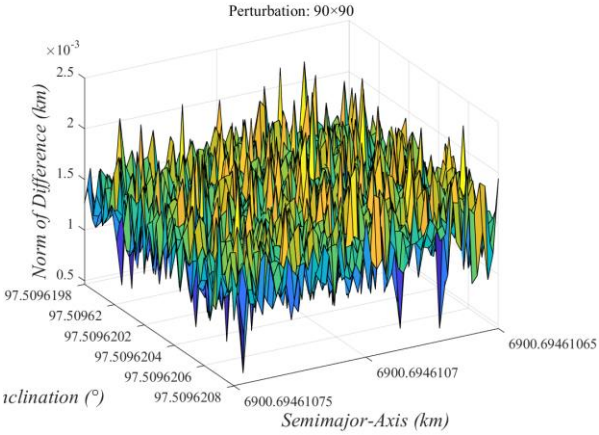

Fig. 5. Distribution Surface under 90 ×90 Perturbation (zoomed to small scale)

However, in practical engineering design, it is often required to design PRT with higher-order perturbations to minimize the cost of orbital maintenance around the nominal trajectory [7 , 8]. Fig. 3 illustrates the distribution under 90×90 order non-spherical perturbations. The scale shown in the figure is a typical one at the beginning of the 2nd Regression Refinement Phase. It is indicated in the figure that the distribution remains smooth at this level of scale. The scale involved in the 1st Regression Refinement Phase is larger than in this figure. This explains why gradient methods can be applied to the 1st phase. When appropriately magnifying the vicinity of the minimum of this surface, a noisy-like distribution can be observed. This is because during the integral duration of up to several days, high-order harmonic terms and tesseral terms in the satellite's path causes nonlinear changes in the entire integration path and dynamic condition, once starts from a small initial variation. This can also be understood as a chaotic effect. At this scale, gradient methods are no longer applicable.

Subsequently, the vicinity near the minimum is further

magnified, as shown in Fig. 5. The figure illustrates a noteworthy situation. At this scale, most local minima are still greater than 1 meter, so converging only to this level of small scale and to any local minimum is not sufficient. This would still be considered premature termination of the optimization process. In such a distribution, it is understandable that global optimization methods such as GA (Genetic Algorithms), PSO (Particle Swarm Optimization), DE (Differential Evolution), or SA (Simulated Annealing) cannot guarantee convergence to the global minimum. On the other hand, global optimization algorithms are also not feasible due to the need for an extremely large number of evaluations. Therefore, an effective optimization algorithm is required in this work.

B. Description of the Unconstrainted Problem

In some studies [6, 9], the sun-synchronous characteristic needs to be examined and is given attention during the optimization process. In some optimization phases, it is treated as a constraint. However, quantification of sun-synchronous characteristic as a constraint is seldom mentioned by previous studies. On the other hand, the addition of constraints also increases the burden of the optimization process. At very small scales, as discussed in the previous section, it is not easy to converge smoothly to the specified accuracy even without constraints. Therefore, additional discussion of sun-synchronous fulfilments can have a negative impact on the convergence process.

A sun-synchronous orbit is defined as one where, regardless of being at the ascending node, descending node, or any point along the orbit, the satellite remains at the same time of day (mean sidereal time) whenever it is above the same point on the Earth's surface [10]. Take an example of a sun-synchronous orbit with a descending node passage at 08:00 local time. Set the sub-satellite point when the satellite passes the descending node at time 0 as Point A. At this moment, the local time at Point A is 08:00. After several whole days, i.e., one regression period (denoted as time t at this end of this duration), the local time at Point A remains precisely at 08:00. Meanwhile, the satellite completes regression, indicating that the satellite is precisely located at the descending node and at the same location as at time 0. This means there is no change in local time at the descending node of the orbit. This cycle repeats from time t onwards, ensuring that the local time at the descending node of the orbit remains constant.
As a conclusion, for orbits with an integer number of regression period, i.e., of which the integral duration equals an integer number of days, it is not necessary to consider the sun-synchronous factor throughout the entire optimization process. The convergence of the optimization ensures sun-synchronous characteristics.

IV. Multistage Optimization Structure

In Section II, it is mentioned that the problem in this work generally adopts the classical three-stage independent optimization structure. Fig. 6 presents a simulation architecture built upon this classical

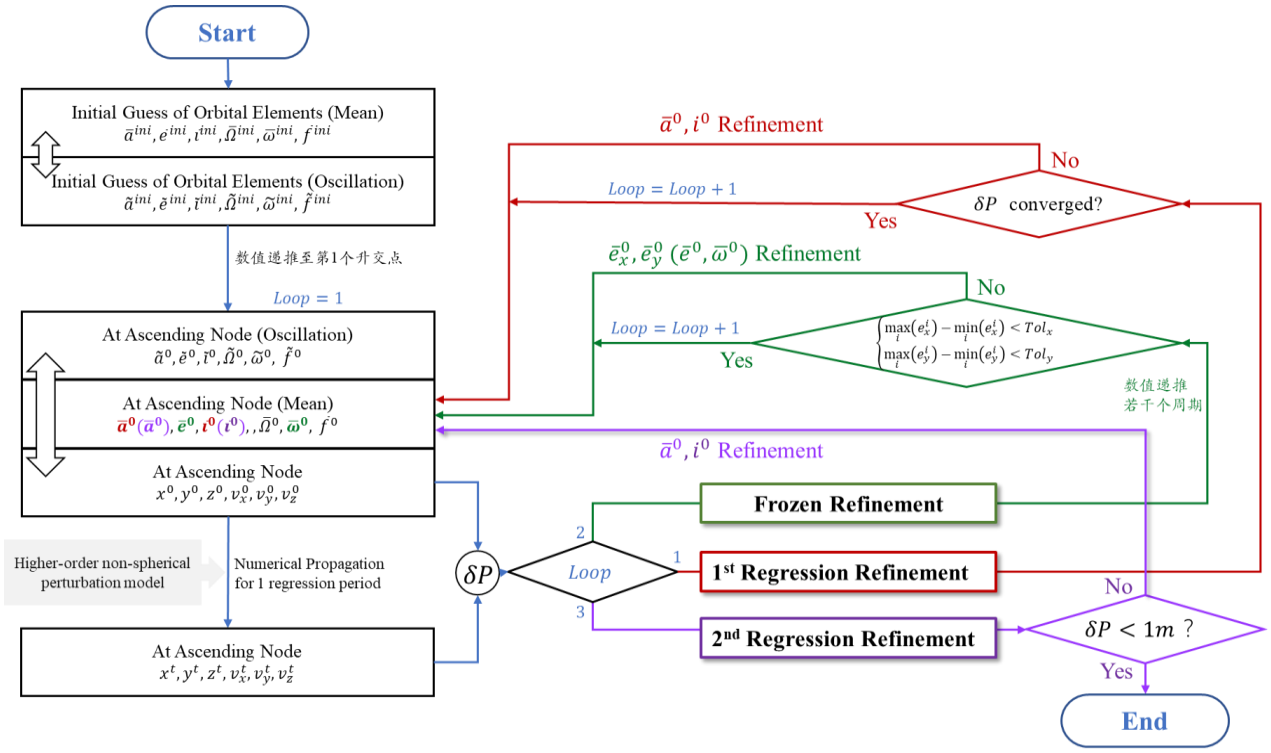

Fig. 6. Simulation Structure Diagram

framework. In this architecture, a set of regression orbital elements is first provided under J2 perturbations. Although it is not essential for sun-synchronous orbits, we still propagate this orbit to the ascending node for ease of data processing and analysis. The mean orbital elements at the ascending node are then taken as the initial guess for optimization. Subsequently, based on this, optimization process is to be conducted in three stages.

A. 1st Regression Refinement & Frozen Refinement

Under a perturbation model of specified order, the semimajor axis and inclination are designed using differential corrections. Iterations are conducted multiple times to ensure that the sub-satellite point trajectory regresses while simultaneously satisfying the requirements for sun-synchronous.

Given the semimajor axis a, inclination i, and other initial orbital elements, the initial orbit is numerically propagated precisely for one regression period. This yields the mapping relationship with longitude and latitude corresponding to its position.

$$[\lambda, \phi] = f(a,i) \tag{3}$$

In the context of J2 perturbation, the above function can be expressed analytically. However, under higher-order perturbations, it can only be obtained through numerical propagation.

The objective function in this phase can also be directly defined with

$$\delta P = f(a,i) \tag{4}$$

Investigations suggest that, regardless of the order of perturbations, the scale in the 1st Regression Refinement Phase is relatively large, making traditional gradient methods such as Newton's method and differential corrections effective for convergence. For details about gradient methods and related algorithms, please refer to [11,12,13].

In the Frozen Optimization Phase, the frozen characteristics is optimized through designing the eccentricity vectors. This allows the orbit to regress in the altitude direction as well [14].

Utilizing the long-term evolution characteristics of eccentricity e and argument of perigee ω under high-precision perturbations, the orbit is numerically propagated for several regression periods to form a closed elliptical curve with eccentricity vector $e_x = e \cdot \cos(\omega), e_y = e \cdot \sin(\omega)$. By iteratively improving the eccentricity vectors $[e_x, e_y]$, the size scale of this curve is reduced. Therefore, the variation amplitude of the eccentricity vector under long-term propagation is suppressed, which ensures regression in the altitude direction.

B. CLASSICAL OPTIMIZATION METHOD for the 2nd Regression Refinement

In the 2nd Regression Refinement Phase, as described in Section III, the gradient methods applied in the 1st Regression Refinement phase are not suitable for the needs of this phase. Therefore, nonlinear optimization tools must be employed for classical methods to optimize to a PRT under higher-order gravity field models [6].

In a fixed-duration orbit, n intermediate points M_1, M_2,…, M_n are set as virtual impulse maneuver points (position continuous, velocity discontinuous) to achieve a smooth connection between the beginning and end of the orbit. Each virtual impulse point has a pre-set epoch time, denoted as T_1, T_2 ,…, T_n. Hence, this problem is described as a system with $7n$ degrees of freedom, subject to constraints: the positions of the intermediate points are the same, and the positions and velocities of the two end points (T_0, T_f) are also the same, with a total of 3n+6 constraints. The objective is to minimize the total virtual impulse velocities at the n intermediate points (reaching zero for smooth trajectory). Therefore, the optimization problem can be written as follows:

$$\min_{T_i, \mathbf{x}_i^p, \Delta\mathbf{v}_i \in \Re^n} \sum_{i=1}^{n} \|\Delta\mathbf{v}_i\|, \quad i = 1, \dots, n \tag{5}$$

subject to

$$\mathbf{x}_i^p(T_i) = \mathbf{x}_{i+1}^p(T_i), \quad i = 1, \dots, n-1 \tag{6}$$

$$\mathbf{x}_{n+1}^p(T_f) = \mathbf{x}_1^p(T_i) \tag{7}$$

$$\mathbf{x}_{n+1}^v(T_f) = \mathbf{x}_1^v(T_i) \tag{8}$$

where

$$\Delta\mathbf{v}_i = \mathbf{x}_{i+1}^v(T_i) - \mathbf{x}_i^v(T_i), \quad i = 1, \dots, n-1 \tag{9}$$

$\mathbf{x}_i^p$ and $\mathbf{x}_i^v$ denotes the position and velocity vectors at the i-th maneuver, separately.

This approach essentially increases the degrees of freedom in the problem, providing a greater chance for convergence in cases where the original problem had a high convergence difficulty. However, there are also several practical considerations to be aware of:

a) The search dimension is high. When n is set to 1, the search dimension is not even higher than the constraint dimension, making the optimization process infeasible. Therefore, n must be at least 2. At this point, the problem dimension is 14, with 12 constraints. This results in significant computational complexity and a complex search process, often requiring specialized optimization tools and imposing certain demands on computational resources.

b) There is currently no relevant research on its convergence reliability.

c) The generated trajectory is not one strictly defined dynamical trajectory. The presence of virtual velocity increments leads to velocity discontinuities at the n intermediate points. Additionally, the accuracy of constraint satisfaction cannot be perfectly equal to zero, leading to minor positional jumps. Consequently, in practical PRT orbital control processes, this can cause abrupt changes in the trajectory evolution within the tube. They are required to be recognized as sudden disturbances or perturbations in trajectory control strategy design and needs to be particularly emphasized and addressed during the design of orbital control strategies.

C. *Nelder-Mead Method for the 2nd Regression Refinement*

To meet the requirements of " Fast Computation and Rapid acquisition" in practical engineering, there is a need for an optimization method with a simpler and more straightforward logic, ensuring reliable convergence.

The Nelder-Mead method, also known as the downhill simplex method, stands as a prominent technique within the domain of optimization, particularly suited for unconstrained optimization tasks. Classified under the category of direct search methods, this approach diverges from conventional methods by eschewing the necessity for derivative information of the objective function. Instead, it leverages a geometric framework centered around a simplex structure — a polytope with n+1 vertices embedded within an n-dimensional space, where n = 2 in this work.

During each iteration, the Nelder-Mead method meticulously evaluates the objective function at the vertices of the simplex and undertakes strategic transformations guided by the function's values. These transformations encompass reflection, expansion, contraction, and shrinkage operations, collectively steering the simplex towards the global minimum of the objective function. For details, refer to [15,16].

V. SIMULATIONS

A 529 km sun-synchronous orbit with 8-day regression is used as a typical case for simulation. The initial setup is presented in Tabel 1.

Tabel 1. Initial Orbit Parameters

Epoch	00:00:00 1 Jan 2023 UTC
Semimajor Axis	6900.763 *km*
Eccentricity	0.001
Inclination	97.5°
RAAN	190.391°
Argument of Perigee	90°
True Anomaly	90°

In the 1st Regression Phase, the convergence accuracy is at kilometer-level. The problem scale is not sufficiently small, so the non-convexity of the response distribution of the objective function is not notable. In this phase, traditional gradient optimization methods can still effectively achieve convergence regardless of the perturbation order.

In the Frozen Refinement Phase, even under high-order perturbations of 90x90, converge can still be achieved to an accuracy level of 10^{-4} km (e_x and e_y), which is sufficient.

As mentioned earlier, similar to the first one, the 2nd Regression Refinement Phase is also an unconstrained two-dimensional optimization problem. Firstly, optimization convergence under a 2x0 perturbation order is conducted. The convergence process is illustrated in Fig. 7, where the horizontal axis represents the total number of evaluations of the objective function, while the vertical axis shows the residual difference after convergence. Each block represents one iteration. The figure indicates that both the Nelder-Mead method and traditional optimization methods utilizing gradient information can converge to the specified accuracy, i.e., within 1 meter.

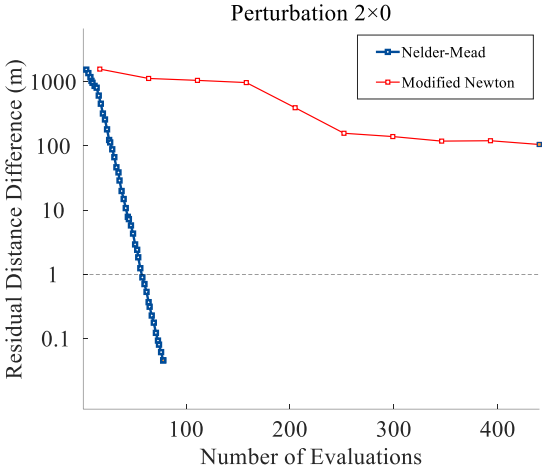

Fig. 7.*Converging history (2 ×0)*

Tabel 2. Comparison of Methods (2×0)

Method	**Convergence residual**	**Number of Evaluations**
Modified Newton	0.05 m	440
Nelder-Mead	0.024 m	75

The convergence residual and the total number of evaluations are also listed in Table 2. From the table, although convergence can be achieved, the Modified Newton method significantly requires more evaluations of the evaluation function compared to the Nelder-Mead method. This is because gradient descent methods require repeated computation of the partial derivative matrix and multiple one-dimensional searches in the

search direction, all of which necessitate multiple executions of the evaluation function.

Next, the convergence behaviour by both methods under 90×90 non-spherical perturbation is compared. Notably, in order to compare the different characteristics of convergence at small scales, the processes of the 1st Regression Refinement and the Frozen Refinement in this experiment are exactly the same as those under the 2×0 case. From Fig. *8*, it can be observed that only the Nelder-Mead method successfully converges to the optimal value, while decreasing trend is not shown on traditional gradient methods. As mentioned earlier, the non-linear characteristics of the evaluation function distribution under high-order perturbations lead to an unreliable gradient matrix, resulting in the optimization process not proceeding as expected. In Tabel 3, since the gradient method are not able to converge, its convergence residuals and number of evaluations are not given out.

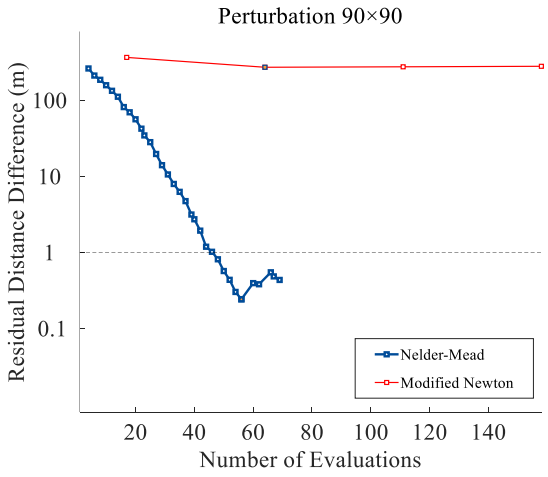

Fig. *8.Converging history (90×90)*

Tabel 3. Comparison of Methods (90×90)

Method	Convergence residual	Number of Evaluations
Modified Newton	/	/
Nelder-Mead	0.24	69

To compare the convergence stability, 40 cases with different initial orbits for optimization calculations are defined. These 40 cases include 10 different orbit altitudes and 4 different right ascension of ascending nodes (RAAN). Among them, the 10 orbit altitudes are all 8-day regressive orbits between 200km and 1000km, demonstrating the suitability of the proposed method for various altitudes of sun-synchronous orbits. The altitudes are specifically 240.791km, 310.180km, 381.417km, 454.580km, 529.752km, 607.021km, 686.489km, 768.256km, 852.426km, and 939.113km. The 4 RAAN values are selected to simulate convergence along different gravity field paths while also representing different local times of descending nodes, specifically 0°, 90°, 180°, and 270°. The other parameters are the same as listed in Tabel 1. The same convergence process as described earlier is performed under each case. Here, "successful convergence" is defined as a convergence residual difference of being less than 1m and keeping in this range for several consecutive iterations.

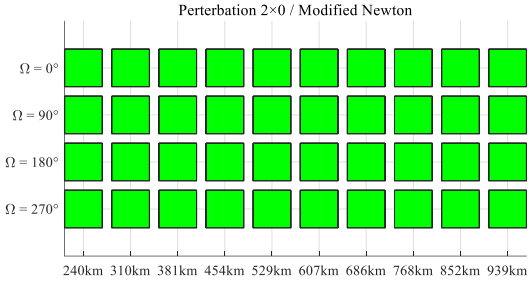

Fig. *9. Converging Success Rate of Modified Newton Method based on 2×0 Perturbation*

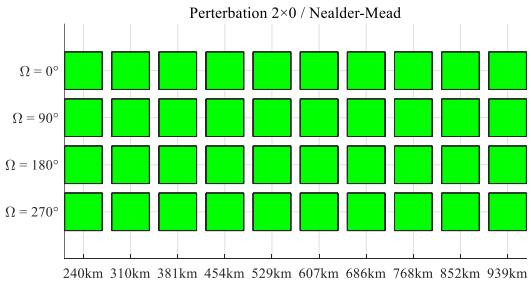

Fig. *10. Converging Success Rate of Nealer-Mead Method based on 2×0 Perturbation*

Fig. *9* and Fig. *10* presents the convergence success or failure of the 40 cases under both methods, respectively. All cases in the figures are indicated in green, indicating that they all converged successfully to the specified accuracy of less than 1m. As mentioned earlier, in the case of low-order perturbations, all methods are applicable.

Expanding the above experiments to higher-order perturbations, significant differences between the methods can be easily observed. Fig. *11* and Fig. *12* compare two methods under 90×90 order non-spherical perturbations. In Fig. *11*, red squares represent cases where convergence totally failed, while yellow boxes represent cases where the stable state to somewhat extent was reached but the results does not meet the 1m accuracy requirement. It is evident from the graph that the gradient method has a significantly lower success rate in convergence. Fig. *12* indicates that the Nelder-Mead method can still converge stably to the specified accuracy for all initial conditions even under high-order gravity fields.

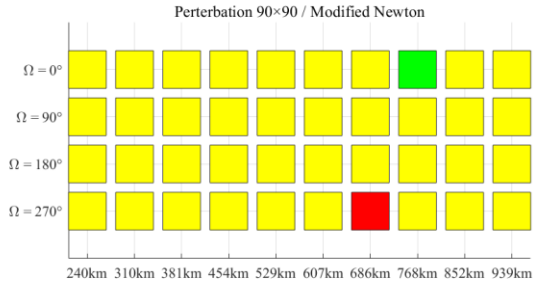

Fig. 11. *Converging Success Rate of Modified Newton Method based on 90×90 Perturbation*

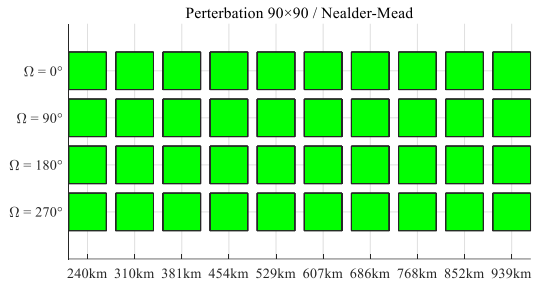

Fig. 12. *Converging Success Rate of Nealer-Mead Method based on 90×90 Perturbation*

VI. CONCLUSIONS

This paper outlined the optimization architecture and process for PRT. Considering that an integer-day regressive orbit is a sufficient condition for meeting the sun-synchronous characteristics, the problem is described as a simple unconstrained two-dimensional optimization problem. This avoids complex large-scale optimization processes and reduces the requirements on the optimizer itself. The Nelder-Mead algorithm is applied in the final stage of the optimization process。

Simulations shows that this algorithm can adapt well even under irregular response distributions caused by high-order perturbations. Moreover, in terms of numbers of evaluation, the Nelder-Mead algorithm reliably achieves convergence with significantly fewer evaluation times compared to traditional gradient methods in cases where convergence is achieved. Unlike other studies that have only provided a single case, this research has presented multiple cases to demonstrate that the algorithm can consistently and effectively converge to the specified accuracy under various conditions. This has significant implications for practical engineering applications.

Future works are as follows,

a) It is worth noting that there are hyperparameters in Nelder-Mead algorithm. Hyperparameters can be improved to make the convergence process more aggressive in the initial stages and adaptively conservative in the final small-scale stages. After training these parameters, it is expected that the optimization efficiency can be further improved.

b) Adaptability of this method in non-sun-synchronous orbits needs to be validated. In non-sun-synchronous orbits, the integral duration is no longer an integer number of days but a complex function related to the semi-major axis and some other factors. The combination of the proposed method and the integration process terminated by events is worthy to be explored.

VII. REFERENCES

[1] I. Barat, P. Prats-Iraola, B. Duesmann, and D. Geudtner, “Sentinel-1: Link Between Orbit Control and Interferometric SAR Baselines Performance,” *25th International Symposium on Space Flight Dynamics*. Munich: German Space Operations Center (GSOC), pp. 19-23, 2015.

[2] R. Kahle, S. Spiridonova, M, Kirschner. “Improved Reference Orbits for The Repeat-Ground-Track Missions EnMAP and Tandem-L,” *Transactions of the Japan Society for Aeronautical and Space Sciences, Aerospace Technology*, vol. 17(3), pp. 308-314, 2019.

[3] M. Lara, and R. P. Russell, “Fast Design of Repeat Ground Track Orbits in High-Fidelity Geopotentials,” *The Journal of the Astronautical Sciences*, vol. 56(3), pp.311-324, 2008.

[4] R. Werninghaus, and S. Buckreuss. “The TerraSAR-X Mission and System Design,” *IEEE Transactions on Geoscience and Remote Sensing*, vol. 48(2), pp.606-614, 2009.

[5] M. Shimada, T. Take, and A. Rosenqvist. “Advanced Land Observing Satellite (ALOS) and Monitoring Global Environmental Change,” *Proceedings of the IEEE*, vol. 98(5), pp.780-799, 2009.

[6] S. D'Amico, C. Arbinger, M. Kirschner, and S. Campagnola, “Generation of an Optimum Target Trajectory for The TerraSAR-X Repeat Observation satellite,” *18th International Symposium on Space Flight Dynamics*, vol. 548, p.137, 2004.

[7] S. De Florio, and S. D’Amico. “Optimal autonomous orbit control of a remote sensing spacecraft,” *Spaceflight Mechanics*, vol. 134, pp. 949-968.

[8] T. Yamamoto, Y. Arikawa, Y. Ueda, H. Itoh, Y. Nishida, H. Tsuru, S. Ukawa, M. Yamamoto, “ALOS-2 autonomous orbit control-one-year experience of flight dynamics operation,” *Proc. 25th Int. Symp. Space Flight Dyn.*, 2015.

[9] M. Kirschner, S. D’Amico, “Generation of the TerraSar-X Reference Orbit,” DLR GSOC TN 04-06.

[10] DT Sandwell, “The Gravity Field of the Earth - Part 1”, 2002.

[11] J. Nocedal, and S. J. Wright, "Numerical Optimization (2nd ed.)," *Springer Science & Business Media*, New York, 2006

[12] S. Ruder. "An overview of gradient descent optimization algorithms," *arXiv preprint arXiv:1609.04747*, 2016.

[13] L. Bottou, "Large-scale machine learning with stochastic gradient descent," *Proceedings of COMPSTAT'2010: 19th International Conference on Computational Statistics*, Paris France, 22-27, August, 2010.

[14] M. Rosengren. "Improved technique for passive eccentricity control," *Orbital Mechanics and Mission Design*, pp. 49–58, 1989.

[15] J. C. Lagarias, J. A. Reeds, M. H. Wright, and P. E. Wright, "Convergence properties of the Nelder--Mead simplex method in low dimensions," *SIAM Journal on optimization*, vol. 9(1), pp. 112-147, 1998.

[16] J. A. Nelder; R. Mead, "A simplex method for function minimization," *Computer Journal*, vol. 7(4), pp. 308–313, 1965